

# Matter-wave bright solitons in spin-orbit coupled Bose-Einstein condensates

V. Achilleos,<sup>1</sup> D. J. Frantzeskakis,<sup>1</sup> P. G. Kevrekidis,<sup>2</sup> and D. E. Pelinovsky<sup>3</sup>

<sup>1</sup>*Department of Physics, University of Athens, Panepistimiopolis, Zografos, Athens 15784, Greece*

<sup>2</sup>*Department of Mathematics and Statistics, University of Massachusetts, Amherst MA 01003-4515, USA*

<sup>3</sup>*Department of Mathematics, McMaster University, Hamilton, Ontario, Canada, L8S 4K1*

We study matter-wave bright solitons in spin-orbit (SO) coupled Bose-Einstein condensates (BECs) with attractive interatomic interactions. We use a multiscale expansion method to identify solution families for chemical potentials in the semi-infinite gap of the linear energy spectrum. Depending on the linear and spin-orbit coupling strengths, the solitons may resemble either standard bright nonlinear Schrödinger solitons or exhibit a modulated density profile, reminiscent of the stripe phase of SO-coupled repulsive BECs. Our numerical results are in excellent agreement with our analytical findings, and demonstrate the potential robustness of such solitons for experimentally relevant conditions through stability analysis and direct numerical simulations.

PACS numbers: 05.45.Yv, 03.75.Lm, 03.75.Mn

*Introduction.* Gauge fields are ubiquitous in physics, as they are relevant to the interactions of charged particles with electromagnetic fields [1] or to fundamental interactions in elementary particle physics [2]. Ultracold atomic gases are considered as an excellent candidate where a variety of artificial gauge fields can be realized; see Ref. [3] for a review. Such gauge fields have been recently studied in experiments [4, 5] with binary Bose-Einstein condensates (BECs). Importantly, synthetic magnetic fields can produce spin-orbit (SO) interactions in a BEC consisting of (predominantly) two hyperfine states of <sup>87</sup>Rb, coupled by a Raman laser [5].

SO-coupled BECs with repulsive interactions have become a topic of intense investigations. Different studies have revealed the existence of a “stripe phase” (consisting of a linear combination of plane waves) [6] and phase transitions between it and states with a single plane wave or with zero momentum [7]. The existence of topological structures, such as vortices with [8] or without [9] rotation, Skyrmions [10] and Dirac monopoles [11], as well as self-trapped states (solitons) of an effective nonlinear Dirac equation (NLDE), was also illustrated [12]. While the above studies refer to BECs with repulsive interactions, to the best of our knowledge, SO-coupled BECs with *attractive interactions* have not been studied so far. The latter, is the theme of the present work.

As it is known, attractive BECs can become themselves matter-wave bright solitons [13], i.e., self-trapped and highly localized mesoscopic quantum systems that can find a variety of applications [14]. Here, we demonstrate the existence, stability and dynamics of matter-wave bright solitons in SO-coupled attractive BECs. In particular, starting from the corresponding mean-field model, we consider the nonlinear waves emerging in the semi-infinite gap of the linear spectrum. Similarly to the repulsive interaction case of Ref. [7], we find three distinct states having: (a) zero momentum, (b) finite momentum,  $+k_0$  or  $-k_0$ , and (c) stripe densities formed by the interference of the modes with  $\pm k_0$  momentum. We analytically identify these branches, in very good agreement with our numerical computations, and determine their spin polarizations. We also analyze the stability of these solutions, illustrating that branches (a) and (c) are generically stable, while branch (b) is stable for sufficiently small atom numbers. Hence, these newly emerging matter-wave solitons in SO-coupled BECs

may be well within experimental reach.

*Model.* We consider SO-coupled BECs confined in a quasi-1D parabolic trap, with longitudinal and transverse frequencies  $\omega_x \ll \omega_\perp$ . In this setting, and for equal contributions of Rashba [15] and Dresselhaus [16] SO couplings (as in the experiment of Ref. [5]), the mean-field energy functional of the system is  $E = \int_{-\infty}^{+\infty} \mathcal{E} dx$ , with:

$$\mathcal{E} = \frac{1}{2} (\Psi^\dagger \mathcal{H}_0 \Psi + g_{11} |\psi_\uparrow|^4 + g_{22} |\psi_\downarrow|^4 + 2g_{12} |\psi_\uparrow|^2 |\psi_\downarrow|^2), \quad (1)$$

where  $\Psi \equiv (\psi_\uparrow \ \psi_\downarrow)^T$ , and the condensate wavefunctions  $\psi_\uparrow$  and  $\psi_\downarrow$  are related to the two pseudo-spin components of the BEC. The single particle Hamiltonian  $\mathcal{H}_0$  in Eq. (1) reads:

$$\mathcal{H}_0 = \frac{1}{2m} (\hat{p}_x \mathbb{1} - k_L \hat{\sigma}_z)^2 + V_{\text{tr}}(x) \mathbb{1} + \Omega \hat{\sigma}_x, \quad (2)$$

where  $\hat{p}_x = -i\hbar \partial_x$  is the momentum operator in the longitudinal direction,  $m$  is the atomic mass,  $\hat{\sigma}_{x,z}$  are the usual  $2 \times 2$  Pauli matrices,  $\mathbb{1}$  is the unit matrix,  $k_L$  is the wavenumber of the Raman laser which couples the two atomic hyperfine states,  $\Omega = \sqrt{2} \Omega_R$  is the strength of the Raman coupling, while  $V_{\text{tr}}(x) = m\omega_x^2 x^2 / 2$  is the harmonic trapping potential. Finally, the effective 1D coupling constants in Eq. (1),  $g_{ij} = 2\alpha_{ij} \hbar \omega_\perp$  ( $i, j = 1, 2$ ), are defined by the  $s$ -wave scattering lengths  $\alpha_{ij}$ ; for attractive interactions,  $\alpha_{ij} < 0$ .

Let us measure length in units of the transverse harmonic oscillator length  $a_\perp = \sqrt{\hbar / (m\omega_\perp)}$ , energy in units of  $\hbar\omega_\perp$ , and densities in units of  $2|\alpha_{11}|$ ; furthermore, employing the gauge transformation  $\psi_{\uparrow,\downarrow}(x, t) \rightarrow \psi_{\uparrow,\downarrow}(x, t) \exp(-i\mu t)$ , where  $\mu$  is the chemical potential, we derive from Eq. (1) the following dimensionless equations of motion for  $\psi_{\uparrow,\downarrow}$ :

$$i\partial_t \psi_\uparrow = \left( -\frac{1}{2} \partial_x^2 - ik_L \partial_x + V_{\text{tr}}(x) - |\psi_\uparrow|^2 - \beta |\psi_\downarrow|^2 \right) \psi_\uparrow - \mu \psi_\uparrow + \Omega \psi_\downarrow, \quad (3)$$

$$i\partial_t \psi_\downarrow = \left( -\frac{1}{2} \partial_x^2 + ik_L \partial_x + V_{\text{tr}}(x) - \beta |\psi_\uparrow|^2 - \gamma |\psi_\downarrow|^2 \right) \psi_\downarrow - \mu \psi_\downarrow + \Omega \psi_\uparrow, \quad (4)$$

where  $V_{\text{tr}}(x) = (\omega_x / \omega_\perp)^2 x^2 / 2$ ,  $\beta = |\alpha_{12} / \alpha_{11}|$ ,  $\gamma = |\alpha_{22} / \alpha_{11}|$ , and we have used the transformations  $k_L \rightarrow k_L / a_\perp$  and  $\Omega \rightarrow \Omega \hbar \omega_\perp$ .

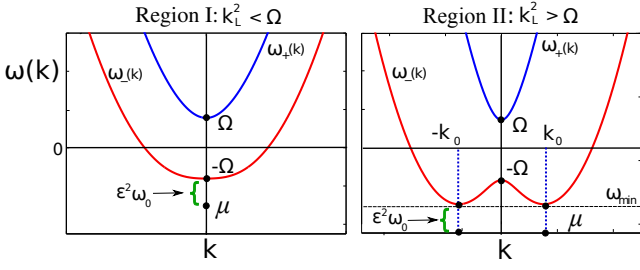


FIG. 1: (Color online) The linear dispersion relation (energy spectrum)  $\omega = \omega_{\pm}(k)$ . The upper branch  $\omega_+$  has a minimum  $(k, \omega) = (0, \Omega)$  in both regions I (left panel) and II (right panel), corresponding to  $k_L^2 < \Omega$  and  $k_L^2 > \Omega$ . The lower branch  $\omega_-$  has a minimum (maximum)  $(k, \omega) = (0, -\Omega)$  in region I (region II); in region II, there also exist two minima  $(\pm k_0, \omega_{\min})$ .

Limiting cases of the system (3)-(4) with  $V_{\text{tr}} = 0$  have been studied in a wide range of contexts. First, in the absence of the kinetic ( $\propto \partial_x^2$ ) and self-interaction ( $|\psi_{\uparrow}|^2 \psi_{\uparrow}, |\psi_{\downarrow}|^2 \psi_{\downarrow}$ ) terms, the above system becomes the massive Thirring model [17], which is a Lorentz-invariant completely integrable system of classical field theory, possessing exact soliton solutions [18]. In the absence of the kinetic terms, but in the presence of self-interactions, the same model has been studied in nonlinear optics; in this case, Eqs. (3)-(4) take the form of a NLDE, which describes solitons in optical fiber gratings [19]. A similar NLDE was also used in the context of SO-coupled BECs [12] and self-trapped states, in the form of gap solitons, were proposed. Finally, a model similar to Eqs. (3)-(4), which includes the kinetic terms with a dispersion coefficient  $D$ , was studied in Ref. [20]; this model, which finds applications to two coupled planar nonlinear optical waveguides, supports so-called “embedded solitons” for various values of  $D$  (and frequency  $\omega$ ); these solitons, however, are generally only semi-stable.

Here, we will use a multiscale expansion method to derive approximate soliton solutions of Eqs. (3)-(4) with a frequency (chemical potential) residing in the semi-infinite gap of the linear spectrum. The solitons will be found to be stable for a wide range of experimentally relevant parameter values. Our analytical results will be obtained for  $\gamma = 1$  and  $V_{\text{tr}} = 0$ ; deviations from this choice will be investigated numerically and they will not qualitatively alter our results.

*Analytical results.* Seeking small-amplitude solutions  $\propto \exp[i(kx - \omega t)]$  of Eqs. (3)-(4) with  $\mu = 0$ , we obtain the following dispersion relation (energy spectrum):

$$\omega_{\pm}(k) = \frac{1}{2}k^2 \pm \sqrt{k_L^2 k^2 + \Omega^2}, \quad (5)$$

which features two distinct branches. The upper branch,  $\omega_+(k)$ , always has a minimum at  $(k, \omega) = (0, +\Omega)$ , and the lower branch,  $\omega_-(k)$ , has different behaviors depending on the sign of the parameter  $\Delta \equiv 1 - k_L^2/\Omega$ : if  $\Delta > 0$  then this branch has a minimum  $(k, \omega) = (0, -\Omega)$  (region I), while if  $\Delta < 0$ ,  $\omega_-(k)$  has a maximum  $(k, \omega) = (0, -\Omega)$  and two minima  $(\pm k_0, \omega_{\min})$  (region II). The dispersion relation  $\omega_{\pm}(k)$  is shown in Fig. 1; clearly, in the linear regime, the lowest energy states in region I can only have zero momentum,  $k = 0$ , while in region II they may have either a positive

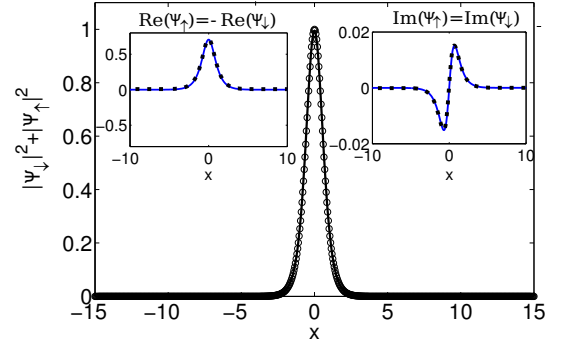


FIG. 2: (Color online) Density profile of the bright soliton in region I. Solid line and circles depict, respectively, the analytical result [pertaining to Eq. (8)] and the numerically found exact solution. Left and right insets show, respectively, the real and imaginary parts of the two wavefunctions. Parameters are:  $k_L = 8$ ,  $\Omega = 120$ ,  $\beta = 0.8$ , and  $\epsilon^2 \omega_0 = 0.4$ .

or negative momentum,  $\pm k_0$ , or they can be a linear superposition of both modes with momentum  $\pm k_0$ , thus forming the “stripe phase” [6].

For  $\mu < -\Omega$  in region I, or  $\mu < \omega_{\min}$  in region II, there exists a semi-infinite gap where linear modes do not propagate. However, matter-wave bright solitons with energies inside the semi-infinite gap can be found analytically via a multiscale expansion method. In particular, let  $\mu = -\Omega - \epsilon^2 \omega_0$  in region I and  $\mu = \omega_{\min} - \epsilon^2 \omega_0$  in region II, where  $\epsilon$  is a formal small parameter and  $\omega_0$  is a free positive parameter (with  $\omega_0/\Omega = \mathcal{O}(1)$ ), which sets the energy difference,  $\epsilon^2 \omega_0$ , from the linear limit inside the semi-infinite gap (cf. Fig. 1). We seek solutions of Eqs. (3)-(4) in the form:

$$\begin{pmatrix} \psi_{\uparrow}(x, t) \\ \psi_{\downarrow}(x, t) \end{pmatrix} = \begin{pmatrix} \epsilon A(X) \\ \epsilon B(X) \end{pmatrix} e^{iKx}, \quad (6)$$

where  $A(X)$  and  $B(X)$  are unknown functions of the slow variable  $X \equiv \epsilon x$ , while the momentum  $K$  is chosen as  $K = 0$  in region I and  $K = \pm k_0$  in region II. Expanding  $A(X)$  and  $B(X)$  as a series in  $\epsilon$ , i.e.,  $A(X) = \sum_{n \geq 0} \epsilon^n a_n(X)$  and  $B(X) = \sum_{n \geq 0} \epsilon^n b_n(X)$ , and substituting the above expressions in Eqs. (3)-(4), we obtain the following.

In Region I, the solvability conditions at the leading [ $\mathcal{O}(1)$ ] and first-order [ $\mathcal{O}(\epsilon)$ ] approximations are satisfied if  $a_0 = -b_0 \equiv u(X)$  and  $a_1 = b_1 = i(k_L/2\Omega)u'(X)$ , where  $u(X)$  is an unknown complex function (primes denote derivatives with respect to  $X$ ). The latter is determined at the order  $\mathcal{O}(\epsilon^2)$ , where the solvability condition is the following stationary nonlinear Schrödinger (NLS) equation:

$$u'' - \lambda u + \nu |u|^2 u = 0, \quad (7)$$

where the positive coefficients  $\lambda$  and  $\nu$  are given by:

$$\lambda = 2\omega_0 \Delta^{-1}, \quad \nu = 2(1 + \beta) \Delta^{-1}$$

(recall that  $\Delta > 0$  in region I).

In region II for  $K = \pm k_0$ , the solvability condition at the leading order reads as a linear equation connecting functions

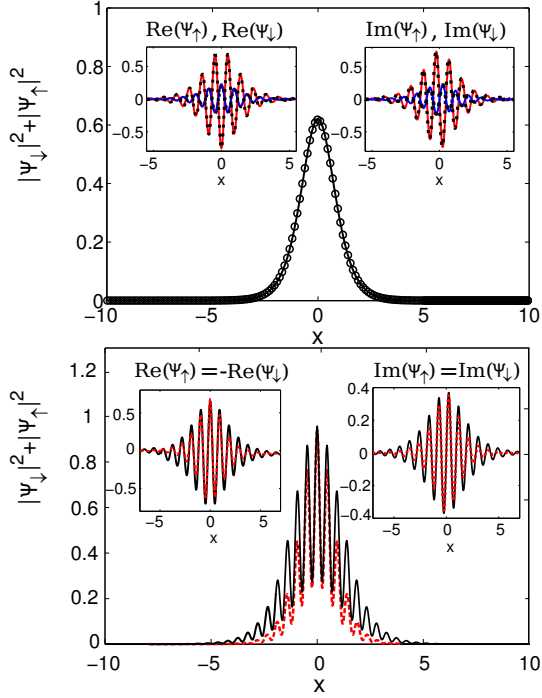


FIG. 3: (Color online) Same as in Fig. 2 but for the solitons in region II. The top and bottom panels show, respectively, the soliton with  $k = +k_0$  [cf. Eq. (9)] and the “stripe soliton” [cf. Eq. (11)]. Parameters used are as in Fig. 2, but with  $\Omega = 35$  and  $\epsilon^2\omega_0 = 0.2$ .

$a_0(X)$  and  $b_0(X)$ , namely

$$a_0 = -\Omega^{-1}k_L(k_L \mp k_0)b_0 = u(X).$$

At the first order, we obtain a similar condition for the functions  $a_1(X)$  and  $b_1(X)$ , namely

$$k_L(k_L \pm k_0)a_1(X) + \Omega b_1(X) = i(k_L \pm k_0)u'(X).$$

Finally, at the order  $\mathcal{O}(\epsilon^2)$ , the solvability condition is again a stationary NLS of the form of Eq. (7), but with the coefficients  $\lambda$  and  $\nu$  now given by:

$$\lambda = \frac{2\omega_0 k_L^2}{k_0^2}, \quad \nu = \frac{2k_L(k_L \pm k_0)(k_L^4 + k_L^2 k_0^2 + \beta\Omega^2)}{\Omega^2 k_0^2}.$$

Taking into regard that the soliton solution of the stationary NLS Eq. (7) is of the form  $u(X) = \sqrt{2\lambda/\nu} \operatorname{sech}(\sqrt{\lambda}X)$ , we end up with approximate [valid up to the order  $\mathcal{O}(\epsilon^2)$ ] soliton solutions of Eqs. (3)-(4) for the wavefunctions  $\psi_{\uparrow,\downarrow}(x, t)$ . These solutions, characterized by the free parameter  $\epsilon\sqrt{\omega_0}$  (measuring the energy difference from the linear regime), have the following form: in region I,

$$\begin{pmatrix} \psi_{\uparrow} \\ \psi_{\downarrow} \end{pmatrix} \approx \epsilon \sqrt{\frac{2\omega_0}{1+\beta}} \operatorname{sech}\left(\epsilon \sqrt{\frac{2\omega_0}{\Delta}} x\right) \begin{pmatrix} 1 \\ -1 \end{pmatrix}, \quad (8)$$

and in region II,

$$\begin{pmatrix} \psi_{\uparrow} \\ \psi_{\downarrow} \end{pmatrix} \approx \frac{\epsilon}{\sqrt{k_L \pm k_0}} f(x) e^{\pm ik_0 x} \begin{pmatrix} \Omega \\ -k_L(k_L \pm k_0) \end{pmatrix}, \quad (9)$$

where the function  $f(x)$  is given by:

$$f(x) = \frac{\sqrt{2\omega_0 k_L}}{\sqrt{k_L^4 + k_L^2 k_0^2 + \beta\Omega^2}} \operatorname{sech}\left(\epsilon \sqrt{\frac{2\omega_0 k_L^2}{k_0^2}} x\right). \quad (10)$$

Notice that Eq. (9) describes two different soliton solutions, each corresponding to the locations  $k = \pm k_0$  of the energy minimum. We can construct still another approximate soliton solution by using the linear combination of the above  $\pm k_0$  soliton states. In particular, Eqs. (3)-(4) for  $\gamma = 1$  are compatible with the symmetry  $\psi_{\uparrow} = -\bar{\psi}_{\downarrow}$  (bar denotes complex conjugate) and the following solution satisfies this symmetry:

$$\begin{pmatrix} \psi_{\uparrow} \\ \psi_{\downarrow} \end{pmatrix} \approx \epsilon f(x) \begin{pmatrix} C_1 \cos(k_0 x) + iC_2 \sin(k_0 x) \\ -C_1 \cos(k_0 x) + iC_2 \sin(k_0 x) \end{pmatrix}, \quad (11)$$

where  $C_1 = \Omega + k_L^2$  and  $C_2 = -k_0 k_L$ . It is clear that, oppositely to the solutions (8)-(9) which have a smooth  $\operatorname{sech}^2$ -shaped density profile, the soliton (11) has a spatially modulated density profile (with a wavelength  $2\pi/k_0$ ); thus, this “stripe soliton” (11) is directly analogous to the characteristic stripe phase of SO-coupled BECs [6, 7], but now for condensates with attractive interactions. Note that only solutions (8) and (11) were considered in the numerical studies of Ref. [20]; solution (9) which does not satisfy the symmetry  $\psi_{\uparrow} = -\bar{\psi}_{\downarrow}$  was not previously explored.

The above solutions describe different spin polarizations of the gas: these are found as the (normalized) longitudinal and transverse spin polarization of the solitons,  $\bar{\sigma}_{x,z} = \langle \sigma_x \rangle / n_{\text{tot}}$ , where  $\langle \sigma_{x,z} \rangle \equiv \Psi^\dagger \hat{\sigma}_{x,z} \Psi$  and  $n_{\text{tot}} = |\psi_{\uparrow}|^2 + |\psi_{\downarrow}|^2$  is the total density. Then, in region I, we find that the solitons are fully polarized along the  $x$ -axis, i.e.,  $\bar{\sigma}_x = -1$  (and  $\bar{\sigma}_z = 0$ ). On the other hand, in region II, the stripe soliton has again  $\bar{\sigma}_z = 0$ , while the  $\pm k_0$  soliton states are characterized by a finite  $\bar{\sigma}_z$ , namely  $\bar{\sigma}_z = \mp \sqrt{1 - (\Omega/k_0^2)^2}$  and  $\bar{\sigma}_x = -\Omega/k_0^2$  (with the total mean spin being  $\sqrt{\bar{\sigma}_x^2 + \bar{\sigma}_z^2} = 1$ ). Thus, spin polarizations of the presented solitons bear resemblance to those found for nonlinear states in SO-coupled repulsive BECs [7].

*Stability and Numerical Results.* In our numerical simulations, we have assumed a quasi-1D attractive BEC, confined in a harmonic trap with frequencies  $\omega_x = 2\pi \times 20$  Hz and  $\omega_{\perp} = 2\pi \times 1000$  Hz containing approximately  $10^3$  atoms, and scattering lengths ratios  $1 : 0.8 : 1$  (i.e.,  $\beta = 0.8$ ); additionally, we have considered a fixed value of  $k_L$ , namely  $k_L = 2\pi/\lambda$  with  $\lambda = 804$  nm and varied the parameter  $\Omega$  in the range  $(1 \div 10)E_L$ , with  $E_L = \hbar^2 k_L^2 / 2m$  (with  $m$  being the  $^7\text{Li}$  mass), to identify solutions in region I or region II (such an investigation complies with pertinent experiments with SO-coupled BECs [5]). We have used a fixed-point algorithm, and an initial ansatz pertaining to solutions (8)-(9) for regions I and II, to find respective numerical solutions. Examples are provided in Fig. 2 (for region I) and Fig. 3 (for region II), where the density profiles,  $n_{\text{tot}} = |\psi_{\uparrow}|^2 + |\psi_{\downarrow}|^2$ , as well as the real and imaginary parts (insets) are shown; the analytical results (solid lines) are in excellent agreement with the numerical ones (circles and dashed lines). Furthermore, we have numerically confirmed (results not shown here) the existence of the presented soliton families for  $\gamma \neq 1$ , in a relatively wide range of values, i.e., for  $0.5 \leq \gamma \leq 1.5$ .

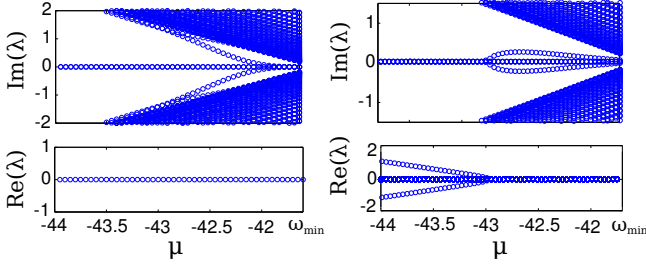


FIG. 4: (Color online) Eigenvalues obtained from the spectral problem (12) for the stripe soliton (left) and  $+k_0$ -soliton (right) branches. The latter becomes spectrally unstable due to the eigenvalue pair with  $\text{Re}(\lambda) \neq 0$  for  $\mu \lesssim -42.9$ . Parameters are as in Fig. 3.

We have also studied the stability of the solitons. Because each solution family corresponds to the energies inside the semi-infinite gap, the spectral stability of solitons is controlled by the negative index count (explained in Ch. 4 of Ref. [21]). Writing the spectral stability problem in the form

$$H\mathbf{u} = i\lambda J\mathbf{u}, \quad (12)$$

where  $\mathbf{u}$  is a  $4 \times 1$  vector of the perturbations to  $[\psi_\uparrow, \bar{\psi}_\uparrow, \psi_\downarrow, \bar{\psi}_\downarrow]$ ,  $H$  is a  $4 \times 4$  self-adjoint matrix operator associated with the right-hand-side of Eqs. (3)-(4) linearized around the solitons,  $J = \text{diag}(1, -1, 1, -1)$ , and  $\lambda$  is a spectral parameter with the instability growth rate given by  $\text{Re}(\lambda)$  (if positive). The operator  $H$  has a finite number of negative eigenvalues, denoted by  $n(H)$ , and a two-dimensional kernel spanned by the symmetries of Eqs. (3)-(4):

$$\mathbf{u}_1 = [i\psi_\uparrow, -i\bar{\psi}_\uparrow, i\psi_\downarrow, -i\bar{\psi}_\downarrow], \quad \mathbf{u}_2 = \partial_x[\psi_\uparrow, \bar{\psi}_\uparrow, \psi_\downarrow, \bar{\psi}_\downarrow].$$

Associated with the eigenvectors of  $H$ , there exist generalized eigenvectors of the spectral stability problem (12) given by solutions of the inhomogeneous equations

$$H\mathbf{v}_j = iJ\mathbf{u}_j, \quad j = 1, 2. \quad (13)$$

Computing the symmetric matrix of symplectic projections with elements  $D_{ij} = \langle \mathbf{v}_i, iJ\mathbf{u}_j \rangle$  ( $i, j = 1, 2$ ), where  $\langle \cdot, \cdot \rangle$  is a standard inner product, we denote the number of negative eigenvalues of  $D$  by  $n(D)$ . The negative index count is now given by  $\# = n(H) - n(D)$  and this number determines the number of unstable eigenvalues with  $\text{Re}(\lambda) > 0$  and/or the number of potentially unstable eigenvalues with  $\text{Re}(\lambda) = 0$  and negative energy in the spectral stability problem (12) [21].

To assess the stability of our solutions, we have computed indices  $n(H)$  and  $n(D)$  for the soliton solutions in region I and II. For solitons in region I and the stripe solitons in region II, we have obtained numerically that  $n(H) = 1$  and  $n(D) = 1$  in their existence intervals, therefore, the negative index  $\#$  is zero. This ensures spectral stability of these solitons. On the other hand, for  $\pm k_0$ -solitons in region II, we have obtained numerically that  $n(H) = 3$  in the existence interval, but  $n(D)$  changes from 1 near the bifurcation at  $\mu = \omega_{\min}$  to 2 for smaller values of  $\mu$ . Therefore, the negative index is  $\# = 2$  near the bifurcation at  $\mu = \omega_{\min}$ , due to a pair of negative

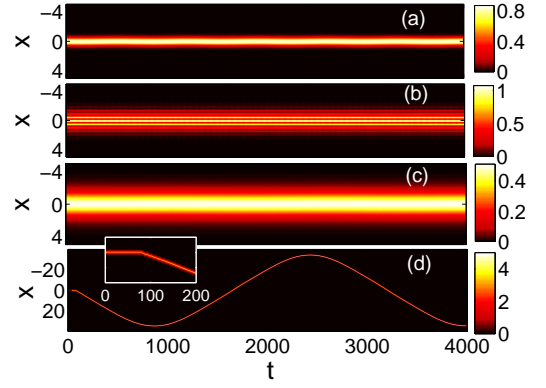


FIG. 5: (Color online) Contour plots showing the evolution of the total density for solitons in region I (a) and region II (b)-(d). Panel (b) corresponds to stripe soliton, while panels (c) and (d) correspond to  $+k_0$ -solitons with  $\mu = -41.77 > \mu_c$  and  $\mu = -43 < \mu_c$  respectively. Other parameters are as in Fig. 2 (but with  $\Omega = 70$ ) and Fig. 3, but now for  $\gamma = 0.8$  and  $\omega_x/\omega_z = 0.02$ .

energy yet neutrally stable eigenvalues in the spectrum of (12). For smaller values of  $\mu$ , it switches to  $\# = 1$  indicating a real unstable eigenvalue.

These results are confirmed by the numerical approximations of eigenvalues in the spectral problem (12). Figure 4 shows the eigenvalues associated with the stripe- and  $+k_0$ -solitons in region II. Spectral stability of the former is contrasted with the potential instability of the latter that arises when a pair of neutrally stable eigenvalues of negative energy crosses zero at  $\mu = \mu_c \approx -42.9$  and splits along the real axis for smaller  $\mu$ , yielding an exponential growth of perturbations.

We have also studied the soliton dynamics for  $\gamma \neq 1$  and in the presence of the trap. We have used our fixed point algorithm to obtain a specific soliton state; then, the numerically found soliton was perturbed by a noise of strength  $\approx 10\%$  of its initial amplitude, and the resulting state was used as initial condition for Eqs. (3)-(4) with the parabolic trap. Results of direct simulations are shown in Fig. 5 for  $\gamma = 0.8$  and trap strength  $\omega_x/\omega_\perp = 0.02$ . Solitons in region I [panel (a)], stripe solitons in region II [panel (b)] and  $k_0$ -solitons with  $\mu = -41.77 > \mu_c$ , corresponding to their stability region [panel (c)], are found to be robust up to  $t = 4000$  (of the order of 1 sec in physical units), which was the time of the simulation. An example of unstable  $k_0$ -solitons with  $\mu = -43 < \mu_c$  is also illustrated [panel (d)]; in this case, the soliton stays quiescent for small times [see inset in panel (d)], but later starts oscillating in the trap due to the onset of the instability.

We stress that although our analytical results were obtained in the case  $\gamma = 1$  and  $V_{\text{tr}} = 0$ , the simulations have revealed the existence and stability of solitons for a wide range of values  $\gamma \neq 1$ , and also in the presence of the trap, as well as for different values of  $\beta$ . This clearly indicates that the presented matter-wave soliton families have an excellent chance to be observed in experiments with SO-coupled attractive BECs.

*Conclusions.* In summary, we have used a multiscale expansion method to identify matter-wave bright soliton states in SO-coupled BECs with attractive interactions. The soli-

tons, which were characterized by a chemical potential residing in the semi-infinite gap of the linear spectrum, were found in analytical form to exhibit either a smooth ( $\text{sech}^2$ -shaped) or a modulated density profile, strongly reminiscent of the stripe phase of SO-coupled repulsive BECs. Our analytical predictions were corroborated by numerical simulations, which have shown that the solitons exist and are generally robust for a wide range of the physical parameters involved (including

chemical potential, interatomic interaction strengths and the presence of trapping potentials), even in the presence of noise. It would be particularly interesting to explore higher dimensional generalizations of such solitary waves and the potential of collapse type phenomenology [22] for the various solitonic phases discussed above. Naturally, also, experimental realizations of such SO-coupled attractive interaction BECs would shed considerable light into such investigations.

- 
- [1] J. J. Sakurai, *Modern quantum mechanics* (Addison-Wesley, Redding, 1994).
- [2] M. E. Peskin and D. V. Schroeder, *An introduction to quantum field theory* (Westview Press, Boulder, 1995).
- [3] J. Dalibard, F. Gerbier, G. Juzeliūnas, and P. Öhberg, *Rev. Mod. Phys.* **83**, 1523 (2011).
- [4] Y.-J. Lin, R. L. Compton, K. Jimenez-Garcia, J. V. Porto, and I. B. Spielman, *Nature* **462**, 628 (2009).
- [5] Y.-J. Lin, K. Jimenez-Garcia, and I. B. Spielman, *Nature*, **471**, 83 (2011).
- [6] T. L. Ho and S. Zhang, *Phys. Rev. Lett.* **107**, 150403 (2011); S. Sinha, R. Nath, and L. Santos, *Phys. Rev. Lett.* **107**, 270401 (2011).
- [7] Y. Li, L. P. Pitaevskii, and S. Stringari, *Phys. Rev. Lett.* **108**, 225301 (2012).
- [8] X.-Q. Xu and J. H. Han, *Phys. Rev. Lett.* **107**, 200401 (2011).
- [9] J. Radić, T. A. Sedrakyan, I. B. Spielman, and V. Galitski, *Phys. Rev. A* **84**, 063604 (2011); B. Ramachandhran, B. Opanchuk, X.-J. Liu, H. Pu, P. D. Drummond, and H. Hu, *Phys. Rev. A* **85**, 023606 (2012).
- [10] T. Kawakami, T. Mizushima, M. Nitta, and K. Machida, *Phys. Rev. Lett.* **109**, 015301 (2012).
- [11] G. J. Conduit, *Phys. Rev. A* **86**, 021605(R) (2012).
- [12] M. Merkl, A. Jacob, F. E. Zimmer, P. Öhberg, and L. Santos, *Phys. Rev. Lett.* **104**, 073603 (2010).
- [13] K. E. Strecker, G. B. Partridge, A. G. Truscott and R. G. Hulet, *Nature* **417**, 150 (2002); L. Khaykovich *et al.*, *Science* **296**, 1290 (2002); S. L. Cornish, S. T. Thompson, and C. E. Wieman, *Phys. Rev. Lett.* **96**, 170401 (2006).
- [14] T. P. Billam, A. L. Marchant, S. L. Cornish, S. A. Gardiner, and N. G. Parker, arXiv:1209.0560.
- [15] Y. A. Bychkov and E. I. Rashba, *J. Phys. C* **17**, 6039 (1984).
- [16] G. Dresselhaus, *Phys. Rev.* **100**, 580 (1955).
- [17] W. E. Thirring, *Ann. Phys. (N.Y.)* **3**, 91 (1958).
- [18] S. J. Orfanidis and R. Wang, *Phys. Lett. B* **57**, 281 (1975); S. J. Chang, S. D. Ellis, and B. W. Lee, *Phys. Rev. D* **11**, 3572 (1975); S. Y. Lee, T. K. Kuo, and A. Gavrielides, *Phys. Rev. D* **12**, 2249 (1975).
- [19] D. N. Christodoulides and R. I. Joseph, *Phys. Rev. Lett.* **62**, 1746 (1989); A. Aceves and S. Wabnitz, *Phys. Lett. A* **141**, 37 (1989).
- [20] A. R. Champneys, B. A. Malomed, and M. J. Friedman, *Phys. Rev. Lett.* **80**, 4169 (1998).
- [21] D. E. Pelinovsky, *Localization in periodic potentials: from Schrödinger operators to the Gross-Pitaevskii equation* (Cambridge University Press, Cambridge, 2011).
- [22] C. Sulem and P. L. Sulem, *The Nonlinear Schrödinger Equation* (Springer-Verlag, New York, 1999).